01 May 2009

Feasibility of Coherent xuv Spectroscopy on the 1S-2S Transition in Singly Ionized Helium

Maximilian Herrmann

Martin K. Haas

Ulrich D. Jentschura
Missouri University of Science and Technology, ulj@mst.edu

Franz Kottmann

et. al. For a complete list of authors, see https://scholarsmine.mst.edu/phys_facwork/828

Recommended Citation

M. Herrmann and M. K. Haas and U. D. Jentschura and F. Kottmann and D. Leibfried and G. Saathoff and C. Gohle and A. Ozawa and V. Batteiger and S. Knunz and N. N. Kolachevsky and H. A. Schussler and T. W. Hansch and T. H. Udem, "Feasibility of Coherent xuv Spectroscopy on the 1S-2S Transition in Singly Ionized Helium," *Physical Review A - Atomic, Molecular, and Optical Physics*, vol. 79, no. 5, pp. 052505-1-052505-15, American Physical Society (APS), May 2009.
The definitive version is available at https://doi.org/10.1103/PhysRevA.79.052505

Feasibility of coherent xuv spectroscopy on the 1*S*-2*S* transition in singly ionized helium

M. Herrmann,[1] M. Haas,[2] U. D. Jentschura,[3] F. Kottmann,[4] D. Leibfried,[5] G. Saathoff,[1] C. Gohle,[1] A. Ozawa,[1] V. Batteiger,[1] S. Knünz,[1] N. Kolachevsky,[1,*] H. A. Schüssler,[6] T. W. Hänsch,[1,7] and Th. Udem[1]

[1]*Max-Planck-Institut für Quantenoptik, 85748 Garching, Germany*

[2]*Department of Diagnostic Radiology, Medical Physics, University Hospital Freiburg, 79095 Freiburg, Germany*

[3]*Department of Physics, Missouri University of Science and Technology, Rolla, Missouri 65409-0640, USA*

[4]*Institut für Teilchenphysik, ETH Zürich, 8093 Zürich, Switzerland*

[5]*National Institute of Standards and Technology, Boulder, Colorado 80305-3328, USA*

[6]*Department of Physics, Texas A&M University, College Station, Texas 77843, USA*

[7]*Ludwig-Maximilians-Universität München, 80539 München, Germany*

(Received 5 August 2008; revised manuscript received 20 February 2009; published 11 May 2009)

The 1*S*-2*S* two-photon transition in singly ionized helium is a highly interesting candidate for precision tests of bound-state quantum electrodynamics (QED). With the recent advent of extreme ultraviolet frequency combs, highly coherent quasi-continuous-wave light sources at 61 nm have become available, and precision spectroscopy of this transition now comes into reach for the first time. We discuss quantitatively the feasibility of such an experiment by analyzing excitation and ionization rates, propose an experimental scheme, and explore the potential for QED tests.

DOI: 10.1103/PhysRevA.79.052505 PACS number(s): 32.30.Jc, 32.80.Fb, 32.80.Wr, 37.10.Ty

I. OVERVIEW

The study of simple hydrogenic systems has played a central role in the development of physics. Theory is highly developed for such systems and can provide extremely accurate predictions to be compared with high-precision experimental data. Prominent tests of bound-state quantum electrodynamics (QED) include, e.g., two-photon spectroscopy on atomic hydrogen [1,2], g factor measurements on hydrogenlike carbon [3] and oxygen [4], or the study of exotic systems such as positronium [5] or muonium [6].

The 1*S*-2*S* two-photon transition in singly ionized helium (Fig. 1) is a sharp resonance in a hydrogenic system (linewidth $\Gamma=84$ Hz [7]; quality factor $Q=1.2\times10^{14}$) that extends the list of simple bound systems which have high potential to accurately test fundamental theories. Especially in comparison to the very successful QED tests in hydrogen 1*S*-2*S* spectroscopy, it reveals its strengths: QED corrections of higher order, which are currently of great interest, scale in hydrogenic systems with large powers of the nuclear charge Z. An example is given by higher-order two-loop self-energy corrections of order $\alpha^2(Z\alpha)^6$, where α denotes the fine-structure constant. The transition energy scales as Z^2; hence, the sensitivity to the interesting higher-order corrections is up to an order of magnitude larger. Further, since the ^{4}He nucleus carries no angular momentum, the centroid frequency is measured directly. Most importantly, He^+ is a charged particle and therefore may be trapped and (sympathetically) cooled in a radio-frequency or Penning trap. As demonstrated in Ref. [8], this allows one to prepare a cold ($T\lesssim20$ mK) sample of helium ions, subject to low systematic uncertainties such as second-order Doppler shifts, collisional shifts, and time-of-flight broadening, and is thus ideally suited for high-precision spectroscopy.

Driving the 1*S*-2*S* transition in He^+ requires radiation at 61 nm. The recently demonstrated extensions of (near-infrared) frequency combs into the extreme ultraviolet (xuv) spectral region [9,10] represent the first coherent narrowband sources for this wavelength. These first-generation sources, however, produced only 1 nW or less average power per harmonic in the xuv region. But we are witnessing rapid progress and current systems can now provide power levels approaching 1 μW [11,12]. In the second part of this paper (Sec. II), we therefore discuss available power levels at 61

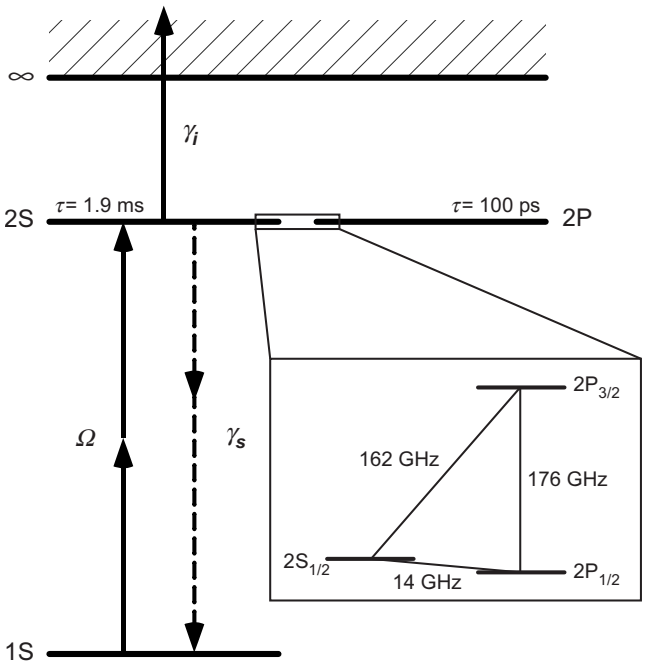

FIG. 1. Relevant energy levels of $^4He^+$. The inset shows the fine structure and Lamb shift of the $n=2$ levels. After two-photon excitation from the ground state, the third ionizing photon reaches 6.8 eV into the continuum.

*Permanent address: P.N. Lebedev Physics Institute, Leninsky Prosp. 53, Moscow, 119991 Russia.

nm and analyze the excitation and ionization dynamics of He^+ for this regime. The analysis shows that spectroscopy of a small number of trapped ions with tightly focused xuv beams is currently the most promising approach. In Sec. III, we propose an experimental scheme for high-precision spectroscopy, and in Sec. IV, we explore its potential accuracy by analyzing expected systematic errors and, finally, in Sec. V, we quantitatively discuss the impact of such an experiment on QED tests.

II. EXCITATION DYNAMICS

A. xuv frequency combs

The $1S$-$2S$ two-photon resonance at 61 nm in He^+ (see Fig. 1) lies deep in the extreme ultraviolet about an octave beyond the LiF cutoff ($\sim$120 nm), which marks the shortest wavelength solid materials are transparent to. No continuous-wave (cw) lasers are available in this spectral region, so one has to resort to nonlinear conversion of powerful, typically pulsed, lasers or free-electron lasers. Four-wave mixing and high-harmonic generation (HHG) [13] in gaseous media are the most frequently chosen nonlinear processes. Among these approaches, HHG of a near-infrared femtosecond frequency comb is a particularly favorable approach for precision spectroscopy. Frequency combs excite two-photon transitions much like cw lasers and at the same time exhibit high peak intensities, which makes them well suitable for nonlinear conversion. This was recognized by Baklanov and Chebotaev [14] as early as 1976. They showed that the excitation of a two-photon transition with two counterpropagating frequency combs is equivalent to an excitation with a cw laser of the same average power, provided the pulses are transform limited and the comb mode spacing is at least twice as large as the linewidth of the transition [15]. This remarkable fact may be exemplified by considering a two-photon resonance ν_0 interacting with two anticollinearly propagating pulse trains, whose mode frequencies are given by the frequency-comb equation [16] $f_n = nf_r + f_c$, where f_n is the frequency of the nth mode of the comb, f_r is the repetition frequency, and f_c is the carrier-envelope offset frequency. If two photons from a mode f_{n_0} are in resonance $2(n_0 f_r + f_c) = \nu_0$ with the transition, then this is also the case for all other pairs of modes that lie symmetrically around $f_{n_0} = \nu_0/2$, for example, the sum of a red- and a blue-detuned mode, $(n_0 - 1)f_r + f_c + (n_0 + 1)f_r + f_c = \nu_0$. It can be shown [14] that for a transform-limited pulse all the modes add coherently and so the power of the entire comb contributes to the excitation of the transition. The effective linewidth is given by the linewidth of an individual comb mode, which can ultimately be as narrow as the best cw lasers [17], and not by the pulse bandwidth. Further, the ac Stark shift of the transition, an important systematic uncertainty, scales with the average power, not the peak power [18]. When the comb is scanned across the resonance, the spectrum repeats itself every half repetition rate, hence the requirement that the transition linewidth must be less than half the repetition rate. The main difference to the cw case is that the k vectors of the comb modes do not necessarily all cancel each other. For an atom excited by counterpropagating, but otherwise identical pulses, this does not cause a net shift but can lead to a broadening of the line. For unbound atoms this can be understood in the time domain as time-of-flight broadening because the duration of simultaneous interaction of moving atoms with the counterpropagating pulses is limited by the pulse-collision volume, which in turn is inversely proportional to the pulse bandwidth. Trapped atoms or ions can be localized within the pulse-collision volume so this effect does not occur. Thus, with respect to two-photon transitions, frequency combs can be regarded as quasi-cw sources allowing for high-resolution spectroscopy [18,19].

Owing to the high peak intensities of femtosecond frequency combs, it is possible to shift the comb from the ir to the xuv spectral region by HHG. This process occurs when atoms interact with a laser field whose peak intensity exceeds 10^{13} W/cm^2 so that the electric field of the laser becomes comparable to the Coulomb field that binds the electron to the nucleus. In this case a small fraction of the electron's wave function can be liberated by tunnel ionization, whereupon it is accelerated in the electric field and finally recombines emitting odd harmonics collinear with the driving laser field. In order to enable direct frequency-comb spectroscopy with these high harmonics, the following conflicting requirements have to be addressed: efficient generation of HHG requires large pulse energies and thus low repetition rates. Spectroscopy on the other hand favors well-separated modes, that is, high repetition rates.

Prior 2005 methods such as chirped-pulse amplification have been used to effectively concentrate a given average power of a laser in fewer pulses per second, thus sacrificing repetition rate for pulse energy. Typical repetition rates that allow for HHG with Ti:sapphire laser systems are in the kilohertz regime and represent a very dense frequency comb which may be considered a continuum unless the modes are stabilized to a linewidth much narrower than 1 kHz and are used to probe very narrow transitions. So far HHG with the highest repetition rate obtained by pulse selection and reamplification made use of regenerative amplifiers and reached 100 kHz [20]. In addition, high harmonics have been produced directly with a Ti:sapphire oscillator at 75 MHz, by exploiting the local field enhancement induced by resonant plasmons within a metallic nanostructure [21]. While the mode spacing would be suitable for high-resolution spectroscopy in both cases, the generated xuv power levels are currently too low for our application.

Currently the most promising route to push the repetition rates for HHG into the megahertz regime while maintaining high efficiency makes use of an enhancement resonator [9,10]. This method is similar to resonantly enhanced second-harmonic generation (SHG) that has been used for many years. However, there are extra requirements that need to be fulfilled in order to resonantly enhance all modes of the frequency comb simultaneously. First, the length of the cavity has to match the repetition rate of the laser and second, the group-velocity dispersion needs to be minimized so that the pulse retains its shape when circulating in the cavity. The collinearly generated high harmonics were extracted by total external reflection from an intracavity sapphire plate oriented at Brewster's angle for the fundamental laser. The frequency-

comb structure is expected to be preserved, which could be confirmed by heterodyne beats with the third harmonic.

We also wish to highlight the dramatic progress that is being made with high-power Yb-fiber lasers. Recent demonstrations achieved up to 68 W average power at a repetition rate of close to 1 MHz [22]. When combined with an enhancement resonator such a system can generate close to 1 μW of xuv power [12]. In fact it may even be conceivable that future systems could be used for high-harmonic generation directly from such a laser oscillator.

Finally, one could use amplified *finite* pulse trains. This approach has been used successfully for xuv spectroscopy on krypton [23,24] and xenon [25]. However, the observed linewidth is limited by the length of the pulse train, and it is challenging to control pulse-to-pulse phase shifts with an accuracy suitable for high-resolution spectroscopy. For this reason an "infinite" pulse train, i.e., a frequency comb, appears advantageous. We therefore limit the discussion in the following to spectroscopy with frequency combs.

B. Power at 61 nm

We assume that the xuv frequency comb is produced by high-harmonic generation in an external enhancement cavity for femtosecond pulses. For our discussion we write the output power as

$$P_{\mathrm{xuv}} = P_{\mathrm{ir}} G \epsilon r. \tag{1}$$

The incident power of the frequency comb, denoted by P_{ir}, is enhanced in an external cavity by a factor G, and converted into the xuv with a single-pass conversion efficiency of ϵ. The latter depends strongly on peak intensity and focusing, so in total P_{xuv} scales highly nonlinearly with P_{ir}. The generated radiation is extracted from the cavity by means of an output coupler of efficiency r. The first-generation setup described in Ref. [9] enhanced $P_{\mathrm{ir}}=700$ mW in the infrared, provided by an oscillator with a repetition rate of $f_r=112$ MHz and a pulse length of $t_p=20$ fs, by a factor $G=54$, resulting in 38 W circulating in the cavity. The stored pulses were converted into the xuv with a single-pass conversion efficiency of $\epsilon=2\times10^{-12}$ for the 13th harmonic at 61 nm. The xuv output coupler had an efficiency of 14% at that wavelength, resulting in roughly 10 pW of power extracted. As we will show in Sec. II D this is orders of magnitude short of obtaining a reasonable transition rate. In this experiment, though, the 13th harmonic was in the cutoff region and far from saturation.

Recently, two "second-generation" systems were reported that are capable of producing xuv power levels approaching 1 μW. In [12] a high-power (10 W) 136 MHz repetition rate Yb-fiber laser source together with a new low-dispersion outcoupling method allowed storage of 2.6 kW of 100 fs pulses. Here, the power in the 17th harmonic at 63 nm was measured to be 54 nW, a 5000-fold improvement over the power at 61 nm reported in [9]. We followed a different strategy [11] and reduced the repetition rate to 10.8 MHz. Together with careful dispersion management [26] this allowed us to observe even higher power levels near 61 nm, namely, 840 nW at the 13th harmonic. When comparing these two results the different wavelengths of the driver pulses need to be taken into account. Although longer wavelengths allow one to push the cutoff to higher energies, the harmonic yield decreases $\propto\lambda^{-x}$, where exponents in the range of $x=3,\ldots,6$ are being discussed [27].

It is clear that more powerful femtosecond oscillators and improved enhancement cavities will lead to higher stored pulse energies and thus to higher xuv power levels. The details of the scaling of the output power as a function of the experimental parameters are quite involved, but as a general guideline we note the following:

(i) The output power of the harmonics scales with a large exponent of the peak intensity. The value of the exponent depends on the experimental parameters and has been measured to be about ~9 for the 11th harmonic in [9].

(ii) Looser focusing increases the interaction volume $\propto w_0^4$ and reduces the adverse Guoy phase shift $\propto w_0^2$, where w_0 is the Gaussian beam waist. In fact, it has been shown that the conversion efficiency scales as $\epsilon\propto b^3\propto w_0^6$ [28], where b is the confocal parameter of the focused ir beam.

(iii) Single-pass conversion efficiencies on the order of 10^{-7} are reported to be typical for HHG in a gas jet using chirped-pulse amplifier (CPA) systems [13], with records reaching up to $\epsilon\sim3\times10^{-4}$ [29] for the 13th harmonic. This shows that even slight improvements can lead to orders of magnitude higher output, owing to the nonlinearity of the process. Generally speaking, the xuv output is maximized by optimizing the system such that an intensity in the range $5\times10^{13}-10^{14}$ W/cm^2 is obtained with the largest possible focus.

For spectroscopy the focused average intensity is the relevant parameter, not the power. Previous experiments have shown that HHG radiation is typically emitted in a (near-) diffraction-limited beam [13]. The high beam quality and the short wavelengths therefore allow tight focusing in principle, but will probably be limited by the surface accuracy of the mirrors used. Typical manufacturer specifications are around $\lambda/10$ at 633 nm [30], which corresponds to only ~λ at 61 nm. Nonetheless, in Ref. [31] the 27th harmonic of a Ti:sapphire femtosecond laser at 29.6 nm was focused down to 1 μm spot size using an off-axis paraboloid with a surface accuracy of $\lambda/8$ at 633 nm. The spot size exceeded the diffraction limit in this case only by less than a factor of 2.

Since virtually all materials absorb significantly around 60 nm, delivering the xuv beam from the source to the He^+ ion with low loss presents a challenging task. First, the diverging xuv beam has to be directed at and focused on the ions. To our knowledge, the highest reflectivity normal-incidence mirrors for 61 nm reported so far are B_4C-Ir multilayers that reflect only about 33% [32]. The use of grazing incidence mirrors reduces losses significantly and also allows tight focusing, but is experimentally more demanding. With arrangements of two orthogonal grazing incidence elliptical mirrors such as the Kirkpatrick-Baez design [33], diffraction-limited focusing of x rays at the 100 nm level has been achieved [34]. Second, from the xuv spectrum generated, one might want to isolate the desired wavelength to suppress ionization and ac Stark shifts from the strong ir and other harmonics. This could be done, e.g., by replacing a beam steering or collimation mirror with a toroidal grating. An

elegant alternative is to place the grating inside the HHG cavity as a replacement for a Brewster window as described above [12]. A thin aluminum foil is an interesting alternative to diffractive optics, which acts as a bandpass in the region of 17–83 nm, although the transmission is very low, only about 10% at 60 nm for 150 nm thickness [35]. Finally we note that if the experiment is performed on trapped ions, as our analysis in Secs. II D and III suggests, two vacuum chambers at unequal pressures need to be connected: An ultrahigh vacuum chamber housing the ion trap ($\leq 10^{-10}$ mbar) and the xuv generation chamber which is at much higher pressure due to the gas jet ($\geq 10^{-6}$ mbar).

Depending on the available xuv power, very simple to highly complex "beam lines" can be thought of. In a simple approach two normal-incidence off-axis paraboloids collimate, direct, and focus the xuv light on the He^+ ions, and a thin aluminum foil provides coarse wavelength selectivity and acts as a physical barrier between the vacuum systems. However, this way only about 1% of the power is delivered to the ion. Sophisticated grazing incidence focusing elements with a windowless connection by differential pumping can improve the efficiency by more than an order of magnitude.

In our calculations we assume transform-limited pulses. However, the xuv pulses may posses a temporally varying carrier phase due to the HHG process itself. The largest contribution is expected to be a negative linear chirp [36]. The impact on the excitation rate depends on the details of the spectral phase and is therefore difficult to predict. In case the effect will turn out to significantly reduce the excitation rate, it is possible to precompensate the spectral phase, e.g., by shaping the ir driver pulse accordingly [37], although this will reduce the achievable peak power in the ir and thus the xuv power.

The 10^4-fold improvement from the first- to second-generation cavity-assisted HHG sources and the highly nonlinear response to the stored power raise hope that further significant improvements can be expected. In total, it does not seem unrealistic to expect time-averaged intensities exceeding 10^7 W/m^2=10 μW/μm^2. For example, P=10 μW focused down to w_0=0.5 μm yields $I=2P/\pi w_0^2$=25 μW/μm^2 on axis.

C. Excitation dynamics

We model the He^+ ion as an open two-level system including spontaneous decay and ionization. The latter is important since any hydrogenic system excited from the ground state to a nS or nD state with two photons may be ionized by a third photon of the same laser field. As explained in Sec. II A we treat the xuv comb as a cw laser with the same time-averaged power [14].

From a master equation for the two-level density matrix ρ, we derive, after applying the rotating wave approximation, the following set of equations for the ground- (ρ_{11}) and excited-state (ρ_{22}) populations and coherences ($\rho_{12}=\rho_{21}^*$; for a detailed discussion, see Ref. [38]):

$$\dot{\rho}_{11} = -\Omega\ \mathrm{Im}(\rho_{12}) + \gamma_s \rho_{22}, \tag{2a}$$

TABLE I. Various physical quantities (two-photon Rabi frequency coefficients, ionization width coefficients, ac Stark coefficients, and spontaneous decay constants), which are related to atomic structure used in the calculations [38] for He^+ 1*S*-2*S* spectroscopy. We follow the conventions of Ref. [38].

β_{12}	2.30164×10^{-6} Hz W^{-1} m^2
β_{ioni}	7.51609×10^{-6} Hz W^{-1} m^2
β_{ac}	1.04236×10^{-5} Hz W^{-1} m^2
γ_s	526.72 rad s^{-1}

$$\dot{\rho}_{12} = -i\Delta\omega\rho_{12} + \frac{i\Omega}{2}(\rho_{11}-\rho_{22}) - \frac{\gamma_i+\gamma_s}{2}\rho_{12}, \tag{2b}$$

$$\dot{\rho}_{22} = \Omega\ \mathrm{Im}(\rho_{12}) - (\gamma_i+\gamma_s)\rho_{22}. \tag{2c}$$

Here, Ω is the two-photon Rabi frequency defined as

$$\Omega = 2(2\pi\beta_{12})I, \tag{3}$$

where β_{12} denotes the squared transition matrix element and I is the total (time-averaged) intensity sampled by the ion (we follow the notational conventions and the normalization of the matrix elements as used in Ref. [38]). The coefficients γ_s and γ_i describe the dampings due to spontaneous decay and ionization losses from the 2*S* state, respectively. We assume that the transition is driven by two laser fields of equal frequency, so the ionization rate reads

$$\gamma_i = 2\pi\beta_{\mathrm{ioni}}I. \tag{4}$$

Here, we once again treat the comb like a cw laser. This is justified by the fact that the ionization cross section varies only slightly over the bandwidth of a typical pulse whose duration is on the order of 10 fs. The detuning $\Delta\omega$ finally is defined as

$$\Delta\omega = 2\omega_L - \omega_{12}, \tag{5}$$

where ω_L is the frequency of the laser field. For a more comprehensive study of the line shape and systematic effects, one can include other contributions from, e.g., the ac Stark shift or the second-order Doppler shift in the detuning. The numerical values related to atomic structure used in the calculations are collected in Table I.

D. Rates

The optical Bloch equations [Eqs. (2a)–(2c)] were solved numerically [39] for zero detuning (neglecting the ac Stark shift) for an average intensity of 10 μW/μm^2 at 61 nm. The excitation and ionization probabilities as a function of interaction time are plotted double logarithmically in Fig. 2. The graph shows a few notable features. First, no Rabi oscillations can be seen, since the system is strongly damped by spontaneous decay and ionization. For sufficiently long interaction times, the He^+ ion will be ionized with unity probability. For short interaction times the curves show a slope of 2 for excitation and 3 for ionization, as expected for a two-photon and a three-photon process, respectively. In view of a

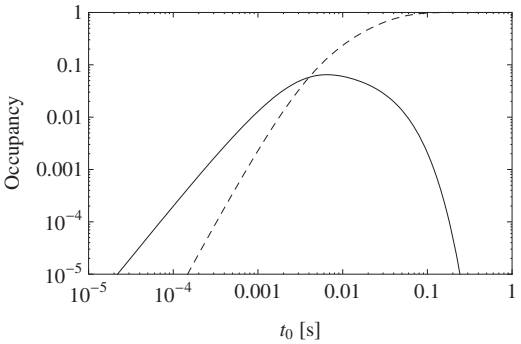

FIG. 2. Excited- (solid line) and ionized-state (dashed line) populations as functions of interaction time t_0 for an He^+ ion illuminated by an average intensity of 10 $\mu W/\mu m^2$ at 61 nm. We describe the $1S$-$2S$ two-photon transition including the ionization channel, as given by Eq. (2), and employ a three-level scheme consisting of the $1S$ ground state, the $2S$ excited state, and a continuum state.

spectroscopy experiment, an important result is that excitation is always accompanied by ionization.

It may be more convenient to express this in terms of "rates." However, this is a poorly defined quantity when dealing with high intensities and/or long interaction times. We therefore define a rate with the following experimental procedure in mind: a single ion interacts with the exciting laser field for a given time t_0. Then, the ions' state is analyzed whereupon the ion is reinitialized and a new cycle begins. In general, there will be a dead time t_d per cycle, e.g., because the excited state needs to be quenched or, in the case of a trapped ion, it needs to be recooled. In total, $f=1/(t_0+t_d)$ experiments may be performed per second. Multiplying f with the excited- or ionized-state occupancy at t_0 given by $[\rho_{22}(t_0)]$ or $[1-\rho_{11}(t_0)-\rho_{22}(t_0)]$, respectively, gives the experimental rates in hertz. For each intensity I and dead time t_d, there is an optimum interaction time $t_0'(t_d,I)$ that maximizes either the excitation or the ionization rate. To give an example, such an optimization is depicted in Fig. 3 for an intensity of 10 $\mu W/\mu m^2$. We use the idealized assumption that there is no dead time; that is, we set $t_d=0$. Therefore, the resulting rates are upper limits on rates that actually may be observed.

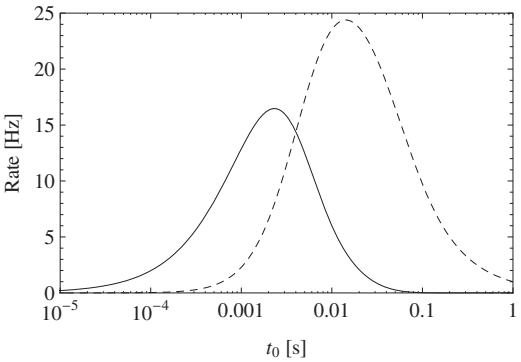

FIG. 3. Optimization of the interaction time t_0 with the exciting laser field to maximize either the excitation rate (solid line) or the resonant three-photon ionization rate (dashed line). The dead time is set to zero and the laser intensity is assumed to be 10 $\mu W/\mu m^2$.

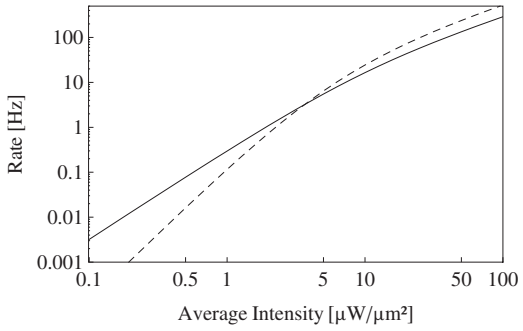

FIG. 4. Excitation (solid line) and resonant ionization rates (dashed line) for a single anticollinearly excited He^+ ion.

To determine the maximum excitation and (resonant) ionization rates as functions of available average intensity, we numerically calculate $t_0'(t_d=0,I)$ and the corresponding rates for a range of intensities as discussed above. The result is shown in Fig. 4. Because we set $t_d=0$, the excitation rate does not saturate at the maximum fluorescence rate given by the lifetime of the $2S$ state in He^+ ($\frac{1}{2}\Gamma=42$ Hz). This limit can indeed be overcome in practice by, e.g., reducing the lifetime of the excited state by a perturbing dc electric field (quenching). In order to put the data plotted in Fig. 4 into perspective, we note that an ionization rate of 1 Hz requires an intensity of 2.3 $\mu W/\mu m^2$, which may be obtained, e.g., by focusing 0.9 μW average power at 61 nm down to $w_0=0.5$ μm.

III. EXPERIMENT

In this section we discuss possible realizations of a precision spectroscopy experiment on the $1S$-$2S$ transition in He^+. The results from Sec. II show that the currently available xuv power levels make tight focusing down to <10 μm and long interaction times necessary to achieve signal rates in the range of ~ 1 Hz. Furthermore, typical xuv pulses have a duration of roughly 100 fs or shorter, which corresponds to a spatial pulse length of (only) ~ 30 μm. If the He^+ ion is excited with anticollinearly propagating pulse trains, the interaction volume (given by the pulse collision-volume) will be very small. These requirements on localization and long interaction times are most conveniently fulfilled by a sample of cold trapped He^+ ions. Therefore, we restrict our discussion for the remainder of this paper to the spectroscopy of a small number of He^+ ions trapped in a linear rf trap.

A. Cooling

Cooling He^+ ions directly is not straightforward. Laser (Doppler) cooling requires a fairly strong (preferably dipole) cycling transition. In He^+, the longest wavelength cycling transition is the $1S$-$2P$ transition at 30 nm. However, no narrow-band (cw) source suitable for cooling is available or in sight for this wavelength [40]. This problem can be solved by introducing a second, easy to cool, ion species into the trap, which sympathetically cools the He^+ ions. The mass of the cooling ions should be as close as possible to the mass of the He^+ ions, (i) to ensure efficient motional coupling and (ii)

to be able to operate the rf trap with convenient parameters. By convenient we mean that the (Mathieu) q parameter of the rf trap is in the range of $0.05<q<0.6$. This dimensionless parameter determines the dynamics of the trapped particle and reads $q=\frac{2QU_{\mathrm{rf}}}{mr_0^2\Omega^2}$, where Q and m are the charge and mass of the ion, U_{rf} and Ω are the rf amplitude and angular frequency and r_0 is the size of the trap, defined as half the distance between (hyperbolic) electrodes. Since q is inversely proportional to the mass, this implies that the cooling ion's mass should be smaller than 48 amu. Therefore, Be^+, Mg^+, and Ca^+ appear to be good choices. Especially Mg^+ is an interesting candidate, since light for the cooling transition near 280 nm can be provided by quadrupling an Yb-fiber laser at 1120 nm in two SHG stages [41].

B. Detection

The vast majority of absolute frequency measurements on single ions utilize shelving (as a "quantum amplifier") [42] in order to detect transitions on narrow lines. Spectroscopy on the $^1S_0$-$^3P_0$ clock transition of Al^+ is a notable exception [43], and methods adopted from quantum computing were used for readout in this case. The He^+ ion also lacks a suitable shelving transition, again because no appropriate 30 nm source is available to date. Direct detection of fluorescence from the $2S$-$1S$ two-photon decay appears not to be viable. The natural fluorescence rate of $\frac{1}{2}\Gamma=42$ Hz is very low in conjunction with typical detection efficiencies of 10^{-3} (including the limited solid angle covered by a typical detector) and photomultiplier dark count rates exceeding 10 Hz. In addition, the two photons emitted by the $2S$ state are in general of unequal wavelength and are, furthermore, not emitted back to back [44]. The situation could be improved by quenching the excited state. This leads to a higher rate and to a well-defined photon energy but on the other hand increases the linewidth and introduces systematic uncertainties. Applying a quantum logic readout scheme similar to the Al^+ experiment would be possible in principle too. But this presents a significant experimental effort (including ground-state cooling) and ionization complicates this approach further. However, the significant ionization probability itself can be utilized to our advantage, that is, for detection. Using the production of He^{2+} ions as signature has the advantageous property that unlike an emitted photon the ion can be stored and detected with an efficiency approaching unity and very low background. Furthermore, it is possible to enhance the expected ionization rate beyond the results discussed in Sec. II D by an additional laser.

In a condensed form, the main steps of our proposed experimental procedure read as follows: (i) trap a cold mixed ion crystal, composed of He^+ and coolant ions; (ii) attempt to excite $1S$-$2S$ with the xuv comb; (iii) if successful, He^{2+} will be produced; (iv) detect He^{2+} by excitation of its unique secular frequency; and (v) step frequency of xuv comb and repeat.

In particular, consider a crystal of two trapped ions, one He^+ and one cooling ion. The ion trap is operated at a (Mathieu) q parameter chosen such that all three involved species, the coolant ion and He^+ and He^{2+}, are within the stability range of the trap. If Mg^+ is used as a coolant ion, this could be realized by choosing, e.g., $q_{Mg^+}=0.05$ and therefore $q_{He^+}=0.3$ and $q_{He^{2+}}=0.6$. The trapped ions oscillate around the trap center with two frequencies: a fast quiver with the trap frequency Ω and a slow charge-to-mass ratio–dependent oscillation, called secular frequency $\omega_s\sim q\Omega/\sqrt{8}$. A successful $2S$ excitation will produce a He^{2+} ion with a certain probability which will (radially) oscillate at twice the secular frequency at which the singly charged He^+ ion did. When we apply an additional perturbing dipolar electric field, we can excite this motion and thus heat the crystal, which in turn will change the fluorescence of the cooling ion. This method, called secular excitation, is routinely used in diagnostics of trapped ions [45]. It might also be sufficient to simply observe a change in the position of the cooling ion due to the He^{2+} ion. A further alternative is to operate the ion trap such that both He^+ and the coolant ion are confined, but He^{2+} will be expelled and can be detected immediately by, e.g., a channeltron.

We would like to emphasize that the proposed detection scheme is essentially background free. If the detection via secular excitation is error free, only very unlikely events can create a false positive. A true positive event, that is, a $Q/m=\frac{1}{4}\frac{e}{u}$ ion disappears and a $Q/m=\frac{1}{2}\frac{e}{u}$ ion appears instead, may be mimicked only by such rare events as the collision of an He^+ ion with an $H_2{}^+$ ion from the background gas, where the He^+ ion is ejected and in exchange the hydrogen molecular ion is trapped. This is important in view of the feasibility of the experiment since the expected signal (ionization) rates are in the hertz range or below, and sensitivity is generally limited by the background.

In the proposed spectroscopy scheme, the clock ions are lost due to ionization, so frequent reloading will be necessary. This could be realized by using a linear trap with multiple segments. Two segments serve as reservoirs and store a large number of He^+ and coolant ions, respectively. Specially designed electrodes transport the ions to a further segment where the two species are merged and the spectroscopy is performed [46], possibly automated by a computer. Alternatively, the He^{2+} ions can be "recycled" to He^+ by purging the trap chamber with a short burst of neutral helium gas. Then, charge exchange collisions of the following type can take place:

$$\mathrm{He}^{2+}+\mathrm{He}\rightarrow 2\mathrm{He}^{+}. \tag{6}$$

The rate of this type of reaction has been determined to be 4.4×10^{-14} cm^3/s for low-energy collisions at 300 K [47]. A charge-exchange rate of 1 Hz thus requires a He pressure of 10^{-3} mbar.

C. Excitation geometry

Due to the low expected transition rate per ion, the question arises as to whether one can take advantage of the large particle numbers ($N\sim10^6$) ion traps can store. Aiming at precision spectroscopy though, only ions in field-free regions of the trap are useful. In a spherical Paul trap this is only one point in space, in a linear trap the axis with no rf confinement. Outside these regions, ions are subject to oscillating

electric quadrupole fields which cause several adverse effects, including ac Stark shifts, second-order Doppler shifts, and a reduction of the lifetime of the excited state by quenching [48]. In the following, we will therefore discuss whether one can benefit from exciting a string of ions in a linear Paul trap rather than working with single ions.

In general, a two-photon transition can be excited either anticollinearly by two counterpropagating photons or collinearly by two copropagating photons. Both processes are described by the same matrix elements, although in the first case the line is free of first-order Doppler and recoil shift, whereas in the second case the line will be broadened and shifted. For unbound atoms excited by counterpropagating beams, this implies that the absorption spectrum consists of a Doppler-broadened pedestal from collinear excitation and a sharp Doppler-free peak in the center. For trapped ions this picture is modified. We will discuss the two contributions separately and also address differences that arise from the orientation of the xuv beams relative to the trap axis, axial or radial.

1. Anticollinear excitation

a. Radial anticollinear excitation. In a radial anticollinear excitation geometry, the xuv beams are oriented antiparallel and perpendicular to the (linear) trap axis. For both collinear and anticollinear radial excitation, simple scaling arguments show that the ionization rate is maximized by focusing down to a single ion. For a three-photon process, the rate scales as $\propto I^3 \propto w_0^{-6}$, where w_0 is the waist size, but the number of interacting ions is proportional to w_0. In total, the rate is thus proportional to w_0^{-5}. Numerical studies outside the regime where this scaling is valid support this statement. The resulting rates are therefore given by the rates for a single ion as shown in Fig. 4.

b. Axial anticollinear excitation. In an axial anticollinear excitation geometry, the xuv beams point along the direction of the axis of dc confinement of the Paul trap, which is parallel to the ion chain. In this case the total rate is enhanced over the radial case simply by the number of He^+ ions in the pulse-collision volume, which is limited by the spatial pulse length and reads $\ell \simeq 2c\tau$, where ℓ is the length of the collision volume and τ is the pulse duration. The number of He^+ ions that can be located in this volume depends on the trapping parameters and cannot be determined analytically. In practice, one considers a given trap with a maximum radial confinement strength described by the radial secular frequency ω_r. To maintain a linear string of ions and prevent breakup into more complicated (e.g., zigzag) structures, the axial confinement ω_{ax} needs to be weaker than the radial by a factor that depends on the number of ions N. This factor has been determined by several authors with different methods, including numerical studies, experimental determinations, and thermodynamical considerations. A recent theoretical result of the latter type which is in good agreement with experimental data reads $\omega_{ax} = \frac{4}{3}\omega_r N^{-1}\sqrt{\ln N}$ [49]. For a given number of ions N and corresponding axial confinement ω_{ax}, the equilibrium positions are then determined numerically by minimizing the potential energy [50]. Figure 5 shows the length of an ion chain as a function of ion number in a rather steep trap with a radial secular frequency of $\omega_r = 2\pi \times 10$ MHz for He^+.

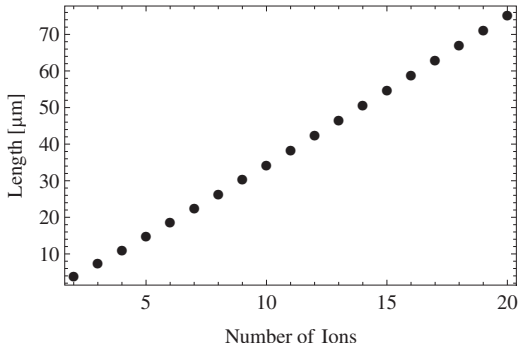

FIG. 5. Numerically determined length l_i of an He^+ ion chain with constant radial confinement of $\omega_r = 2\pi \times 10$ MHz and variable axial confinement to maintain a linear string. The length is well approximated linearly by $l_i \sim N\ 4\ \mu\text{m} - 5\ \mu\text{m}$.

In this case, 30 fs xuv pulses can interact with up to 6 He^+ ions. The length of the chain may of course be reduced by tighter confinement, although one gains only proportional to $\omega_{ax}^{-2/3}$.

From a practical point of view, both radial and axial anticollinear excitations bear great challenges. The signal rate is maximized by tight focusing, so two beams of ~ 1-μm-sized pulses need to be overlapped (i) spatially, (ii) temporally, and (iii) with the He^+ ions. Recall that a repetition rate of, e.g., 100 MHz corresponds to a 3 m pulse-to-pulse separation, so each of the two focusing mirrors may have to be placed 1.5 m away from the ion as low reflective optics inhibit folding the beam.

2. Collinear excitation

For an unbound atom or ion a Doppler-broadened spectrum would be observed, which would limit the spectroscopic accuracy. In the resolved-sideband limit of a trapped ion, the situation is quite different, that is, if the secular frequency of the ion exceeds the linewidth of the transition. In this case, the absorption spectrum consists of a Doppler- and recoil-free carrier with sidebands separated by the secular frequency. All sidebands are of natural linewidth and, for average motional quantum numbers $\bar{n} \gg 1$, lie under an envelope given by Doppler broadening. The center of gravity of the envelope will be shifted by the angular recoil frequency of $\omega_{rec} = \hbar(2k)^2/2m_{He} = 2\pi \times 54$ MHz to the high-frequency side of the spectrum. Note that here as well as in the following, the angular wave number k is multiplied by an extra factor of 2 because two photons are absorbed. The resulting recoil frequency is 2 orders of magnitude larger than in typical spectroscopy experiments on trapped ions, which is the reason why the resulting spectra may appear unfamiliar. Precise spectroscopy can therefore be performed either on the carrier or, if the secular frequency and the order of the sideband are well known, on one of the sidebands. This allows circumvention of the intricate alignment of the xuv beams in anticollinear excitation by simply exciting the He^+ ion with

one xuv beam only. Further, the interaction volume will not be limited by the xuv pulse length anymore, but roughly by the confocal parameter of the focused beam. If, for example, the xuv beam is focused to $w_0=1\ \mu$m the Rayleigh length is $2\pi w_0^2/\lambda=103\ \mu$m. For pulses shorter than 172 fs, this allows one to address more ions simultaneously. The downside is an overall reduction of the rates and an absorption spectrum featuring a larger number of motional sidebands. In the following we will quantify these statements.

The spectrum is calculated as follows. The interaction between the light field and the motional state is characterized by the dimensionless Lamb-Dicke parameter η, which measures the extent of the ion's ground-state wave packet relative to the wavelength

$$\eta = 2kx_0 = 2k\sqrt{\frac{\hbar}{2m\omega_s}} = \sqrt{\frac{\omega_{\mathrm{rec}}}{\omega_s}}. \tag{7}$$

The extent of the ground-state wave packet is denoted by x_0, m is the ion's mass, and ω_s is the secular frequency of the ion. Unlike the usual definition, an extra factor of 2 accommodates the fact that two photons are absorbed. The matrix element for transitions between motional Fock states $|n\rangle$ due to the interaction with the laser reads [51]

$$\begin{aligned}\left|\langle n'|e^{i2k\hat{x}}|n\rangle\right| &= \left|\langle n'|e^{i\eta(\hat{a}+\hat{a}^\dagger)}|n\rangle\right| \\ &= e^{-\eta^2/2}\eta^{|n'-n|}\sqrt{\frac{n_<!}{n_>!}}L_{n_<}^{|n'-n|}(\eta^2),\end{aligned} \tag{8}$$

with the common creation and annihilation operators for the ions' vibration. Further, $n_<=\min(n,n')$, $n_>=\max(n,n')$, and L denotes the generalized Laguerre polynomial. The sideband spectrum is then obtained by summing the squared matrix elements over all possible initial and final states, where the initial states are weighted according to their population [52],

$$\kappa(\Delta\omega) = \sum_{E_n-E_{n'}=\hbar\Delta\omega} \left|\langle n'|e^{i\eta(\hat{a}+\hat{a}^\dagger)}|n\rangle\right|^2 P(n). \tag{9}$$

The sum over all sideband strengths κ equals 1. The effect on the excitation dynamics is to reduce Rabi frequency equation (3) to

$$\Omega = \kappa 2(2\pi\beta_{12})I. \tag{10}$$

The ionization rate remains unchanged. If the ion is in a thermal state, e.g., after cooling, the distribution $P(n)$ reads

$$P(n) = \exp\left(-\frac{n\hbar\omega_s}{k_BT}\right)\left[1-\exp\left(-\frac{\hbar\omega_s}{k_BT}\right)\right], \tag{11}$$

where k_B is the Boltzmann constant.

It is straightforward to generalize this treatment to strings of N ions (closely following Ref. [52]). In a first step, a particular ion string is specified, which can also include cooling ions (e.g., a string consisting of He^+, He^+, Mg^+, He^+). Then, for a given confinement strength, which is specified by the secular frequency of a single ion [which equals the frequency of the center-of-mass (c.m.) mode for an arbitrary number of ions], the positions, eigenmodes β^α, and corresponding eigenfrequencies (secular frequencies) ω_s^α are determined [50]. Here, α enumerates the N eigenmodes. The vector β^α of length N contains the oscillation amplitudes and relative phases of ion j and mode α. Next, the Lamb-Dicke parameter is generalized, so it reads for the jth ion and mode α as

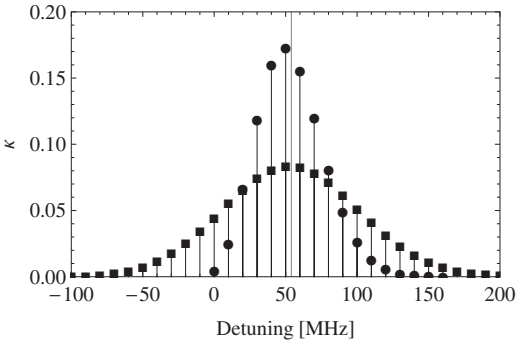

FIG. 6. Sideband spectrum of a collinearly excited He^+ ion with a secular frequency of $\omega_s=2\pi\times10$ MHz. The vertical line indicates the recoil frequency of 54 MHz. Circles and squares indicate whether the ion is assumed to be cooled to the ground state of motion or to 1 mK, respectively.

$$\eta_j^\alpha = 2k\beta_j^\alpha\sqrt{\frac{\hbar}{2m_j\omega_s^\alpha}}. \tag{12}$$

This takes not only the different secular frequencies of the modes into account, but also the various oscillation amplitudes β_j^α, which depend on the mode α and the ion number j. Consider, e.g., the "stretch" mode of a string of three ions of equal mass. In this case, the center ion will be at rest, so its motion will not couple to the light field, as opposed to the outer ions. The motional state vector $|n\rangle$ is replaced by $|\mathbf{n}\rangle=|n_1,n_\alpha,\ldots,n_N\rangle$. With these generalizations, absorption spectra are calculated in close analogy to the single-ion case:

$$\kappa(\Delta\omega) = \sum_{E_n-E_{n'}=\hbar\Delta\omega} \left|\langle \mathbf{n}'|e^{i\eta_j^\alpha(\hat{a}+\hat{a}^\dagger)}|\mathbf{n}\rangle\right|^2 P(\mathbf{n}). \tag{13}$$

The argument of the sum is a product over all eigenmodes α. The sum itself extends over all ions j and combinations of $|n\rangle$ and $|n'\rangle$. For a given trap storing a string of ions one can choose between radial or axial collinear excitation, where "radial" means that the laser propagation direction is perpendicular to the trap axis. It is not immediately clear which orientation yields higher rates.

a. Radial collinear excitation. Figure 6 shows a calculated sideband spectrum of a radially excited tightly confined He^+ ion with a secular frequency of $\omega_s=2\pi\times10$ MHz. In one case it is assumed to be cooled to $T=1$ mK, which corresponds to the Doppler cooling limit of Mg^+. In the other case it is assumed to be cooled to the ground state of motion. As expected, the spectrum of the ion cooled to the ground state is narrower and exhibits stronger individual components. Remarkably, the carrier is stronger for the warmer ion. This is due to the fact that the entire spectrum is shifted by the recoil frequency of $\omega_{\mathrm{rec}}=2\pi\times54$ MHz, because the ion's confinement is weak in comparison to the recoil energy ($\omega_s<\omega_{\mathrm{rec}}$). For very low temperatures, the distribution of

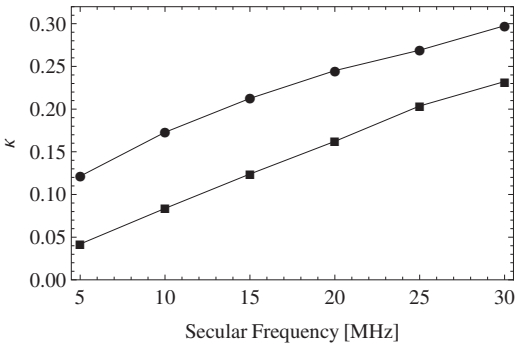

FIG. 7. Relative magnitude of the strongest sideband as a function of secular frequency for He^+ ions cooled to 1 mK (squares) or to the ground state (circles).

sidebands becomes so narrow that the carrier diminishes. For increasing temperatures, the distribution will broaden and flatten so the carrier will become weaker, too. Incidentally, the chosen temperature of 1 mK is near the optimum temperature for which the carrier is maximal ($T_{\mathrm{opt}}=1.3$ mK) for these parameters. In a steeper trap, the absorption spectrum will consist of less and stronger sidebands. In the trap with the highest secular frequencies reported so far [45], $^9Be^+$ ions were confined with secular frequencies of up to 50 MHz. The magnitude of the strongest sideband as a function of the secular frequency is shown for an ion cooled to 1 mK and cooled to the ground state in Fig. 7. We chose the strongest component and not the carrier, since the expected rates are already rather low, and assuming that the secular frequency can be determined sufficiently precise so it will not limit the overall accuracy.

This shows that collinear excitation reduces the Rabi frequency in this example by a factor of 5–10, which has to be compensated for by either five to ten times more xuv power or two to three times tighter focusing to achieve the same rate as in anticollinear excitation.

b. Axial collinear excitation. In this orientation, despite tight focusing, a number of ions can be addressed simultaneously, whose number is in principle only limited by the confocal parameter of the focused xuv beam. On the other hand, as pointed out in Sec. III C 1, the secular frequency is

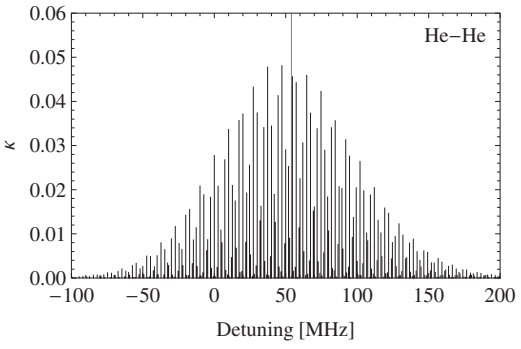

FIG. 8. Sideband spectrum of a string of two axially excited He^+ ions confined with a secular c.m. frequency of 10 MHz and cooled to 1 mK. The vertical line indicates the recoil frequency.

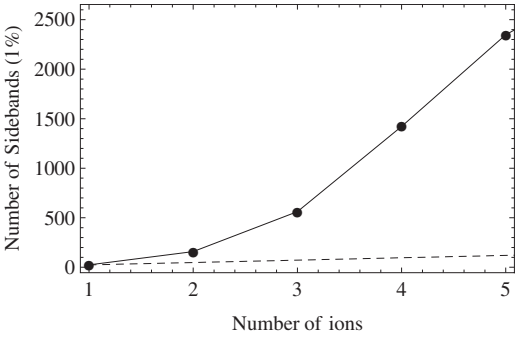

FIG. 9. Calculated number of sidebands that exceed 1% of the strongest component as a function of the number of ions. The secular frequency is 10 MHz; the temperature is 1 mK. The dashed line shows for comparison a hypothetical linear increase in the number of sidebands.

weaker in this direction. For clarity, however, we have studied absorption spectra of ion chains with constant axial trap stiffness, to be able to discriminate the effect of the greater number of ions and the reduced secular frequencies.

Figure 8 shows an absorption spectrum of two He^+ ions cooled to 1 mK with a center-of-mass frequency of 10 MHz. It consists of a rather dense collection of sidebands, none of which is more intense than the strongest component in the spectrum of a single He^+ ion (Fig. 6). This rather counterintuitive result (two ions exhibit no stronger component than a single ion) can be understood as follows: the sum of all sideband strengths in relative units equals the number of ions [53]. But it turns out that if the number of ions is increased, the number of sidebands increases much more rapidly. This is because sidebands are not limited to integer multiples of the N different mode frequencies of the string, as one may tend to expect, but can also occur at sums and differences of integer multiples of the frequencies, as long as energy conservation is fulfilled. In a string of two ions, for example, not only the c.m. *or* the stretch mode can be excited individually, but also any combination. Since the frequencies of the eigenmodes are incommensurate, this results in a dense grid where sidebands can occur in principle. The number of sidebands depends on the definition of how intense a component needs to be to be included. If, for example, all sidebands are counted that exceed 1% of the strongest component, a string of five He^+ ions confined in a $\omega_{\mathrm{c.m.}}=2\pi\times 10$ MHz trap and cooled to 1 mK exhibits 2348 sidebands. This is illustrated in Fig. 9.

We also studied the influence of cooling ions in the string. It turns out that this does not improve the spectrum: the additional cooling ions cause more sidebands without contributing to the signal. An example is shown in Fig. 10 for an ion string consisting of two He^+ and one Mg^+ ion, cooled to 1 mK. As mentioned before, all these spectra have been calculated for constant axial confinement. In a real experiment with given radial confinement, the axial secular frequency needs to be reduced as the number of ions increases to maintain a linear string. The resulting spectra will therefore be even denser with weaker individual components.

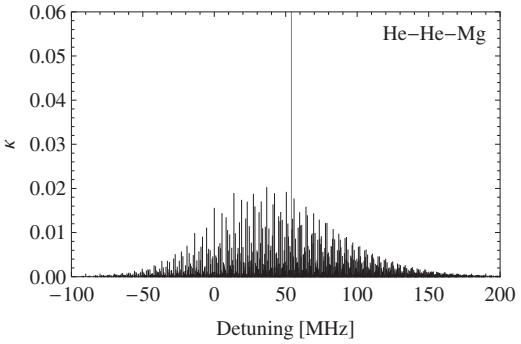

FIG. 10. Same as Fig. 8 except one Mg^+ cooling ion was added.

3. Comparison excitation geometries

From the geometries discussed, axial anticollinear and radial collinear excitations turn out to be the most promising approaches. The anticollinear arrangement yields the highest rates, and if excited axially, on the order of 10 He^+ ions can be addressed simultaneously. The drawback is the possibly intricate alignment of the xuv beams required. Collinear excitation facilitates the alignment significantly, although the Rabi frequency is strongly reduced, and roughly an order of magnitude more xuv power is required to obtain the same rate. Radial collinear excitation of a single ion in a steep trap yields higher rates and clearer spectra than axial collinear excitation of a chain of ions. In all cases, the ionization rate is maximized by tight focusing. In Fig. 11, the scaling of the maximum excitation and ionization rate is shown, recalculated for the case where the Rabi frequency is reduced to 10% by the selection of a particular sideband. The dynamics is slightly different, because the $1S$-$2S$ Rabi frequency is reduced, but the ionization cross section remains unchanged.

For clarity the sideband spectra shown do not take the comb structure of the laser into account. The experimentally observable spectrum is obtained by convolving the spectrum of the xuv comb with the spectrum of the ion. If the width of the absorption spectrum is not significantly narrower than the repetition rate of the comb, this will lead to an even denser spectrum and make it quite challenging to identify the carrier. On the other hand, under certain circumstances, the comb structure of the xuv source can be used to increase the excitation rate. The sidebands of a single collinearly excited He^+ ion form a regular grid with a line spacing given by the secular frequency. If the ratio of the repetition rate of the comb to the secular frequency is rational, it will drive several sidebands simultaneously (all if the ratio is 2).

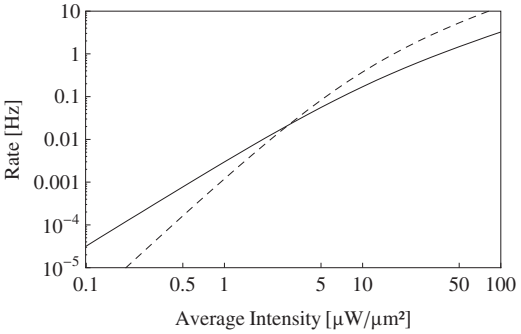

FIG. 11. Maximum excitation (solid line) and ionization rates (dashed line) for one collinearly excited He^+ ion. The Rabi frequency has been reduced to 10%. Since the ionization cross section remains unchanged, the dynamics is slightly different from that in Fig. 4.

IV. SYSTEMATIC UNCERTAINTIES

In order to illustrate the potential accuracy of a high-precision spectroscopy experiment on He^+, we estimate some typical systematic uncertainties. In particular, we assume He^+ ions stored in a rf trap driven with $\Omega = 2\pi \times 60$ MHz and cooled to $T = 1$ mK. The ionic motion due to the finite temperature will cause the line center of the carrier to be shifted by the second-order Doppler effect by

$$\Delta\nu = -\frac{\omega_{12}}{4\pi}\left(\frac{v}{c}\right)^2 = -0.2 \text{ Hz}, \tag{14}$$

where ω_{12} is the $1S$-$2S$ transition frequency. The corresponding fractional frequency shift is 2×10^{-17}.

The secular oscillation of the ion around the trap center causes it to sample an average quadratic electric field, which is calculated by integrating the square of the electric field of the potential up to the classical turning points of the oscillation [48]:

$$\langle E^2 \rangle = \frac{m\Omega^2 k_B T}{e^2} = 51 \times 10^{-3} \text{ V}^2/\text{cm}^2. \tag{15}$$

This leads to a dc Stark shift of [54]

$$\Delta\nu_{\text{dc}} = (3610 \text{ Hz cm}^2/\text{V}^2)\langle E^2 \rangle Z^{-6} = 3 \text{ Hz}, \tag{16}$$

which corresponds to a relative uncertainty of 3×10^{-16} for the electric field given above. The average quadratic electric field will also cause a broadening of the line by reducing the lifetime of the $2S_{1/2}$ state through admixture of the fast-decaying $2P_{1/2}$ state. The lifetime against quenching can easily be calculated by considering the admixture received by the $2S$ state from the $2P$ state, and relating the mixture coefficient to the well-known lifetime of the $2P$ state which decays via a one-photon electric dipole transition to the ground state. The result is

$$\tau' = \frac{0.0158}{\langle E^2 \rangle} \text{ V}^2 \text{ s/cm}^2 = 0.3 \text{ s}. \tag{17}$$

The broadening is only about 0.6% in units of the natural linewidth so that the dynamics calculated above is hardly affected.

The effects discussed so far (second-order Doppler shift, dc Stark shift, and quenching) have been calculated for an ideal trap. Even small stray fields and phase differences between rf electrodes can cause excess micromotion which can increase the uncertainties by orders of magnitude. Great care must therefore be taken to measure and compensate for excess micromotion [48].

The shift due to blackbody radiation (BBR) has recently been calculated to be 0.12 Hz at 300 K [55].

If we assume a time-averaged laser intensity of 10 $\mu W/\mu m^2$, the ac Stark effect shifts the observed line center by

$$\Delta\nu_{ac} = \beta_{ac} I = 100 \text{ Hz}. \tag{18}$$

This contribution is, however, no fundamental limitation, since the measured frequency of the line center can be extrapolated to zero laser intensity after having been recorded for a range of intensities.

Shifts due to external magnetic fields cancel to first order if a $\Delta m=0$ component is measured because the Landé g factors of all S states are identical. However, if we include higher-order corrections we find that the g factors of the ground and excited S states differ slightly. The dominant contribution to the dependence of the g factor on the principal quantum number is given by the following well-known leading term in the $Z\alpha$ expansion of the Breit formula for the bound-electron g factor for S states. This leads to a magnetic-projection-dependent Zeeman energy shift of [56]

$$\Delta E = 2\mu_B B m_J \left[1 - \frac{1}{3}\left(\frac{Z\alpha}{n}\right)^2\right], \tag{19}$$

where μ_B is the Bohr magneton, and $m_J=-\frac{1}{2},\frac{1}{2}$ is the spin projection on the axis of the magnetic field B. This residual Zeeman effect shifts the magnetic field–insensitive components by 0.7 Hz in a field of 10 G, leading to a relative uncertainty of 8×10^{-17}.

It should be pointed out that the $1S$-$2S$ transition is not affected by quadrupole shifts, because neither the ground nor the excited state possesses a quadrupole moment.

With the assumptions made we find the largest systematic line shift to be on the order of 10^{-16} (dc Stark shift). The statistical uncertainty for a known line shape reads

$$\Delta\nu_{1S\text{-}2S} = \frac{\Gamma}{S/N} = \frac{\Gamma}{\sqrt{N_{He^{2+}}}}. \tag{20}$$

The ionization-based detection method proposed above is virtually background free, so the signal-to-noise ratio S/N is limited by the total number of counts $N_{He^{2+}}$, which justifies the last equal sign. The linewidth of the comb modes in the infrared can be stabilized down to 1 Hz [17]. The corresponding linewidth in the xuv region has not been measured yet and depends on the noise processes involved in the HHG process. We assumed in the calculation of the excitation and ionization rates a linewidth of the comb modes narrower than the natural linewidth. Otherwise the rate would be reduced due to poor spectral overlap. For the calculation of the statistical uncertainty we are more pessimistic and conservatively assume a linewidth of 10 kHz. If we further assume an event rate of 0.1 Hz and a measurement time of 10^5 s, then the line center could be determined to within less than 50 Hz, which corresponds to a measurement on the 2×10^{-14} level.

V. IMPACT ON QED

Testing a physical theory means to compare its predictions to experimental findings. The best tests therefore demand a system that can be both measured and calculated with very high accuracy. For a long time the confrontation of transition frequencies in atomic hydrogen with theoretical calculations has allowed for one of the best tests of bound-state QED [1,57]. The $1S$-$2S$ transition plays a prominent role because it possesses a particularly large line quality factor and can be excited in a Doppler-free arrangement with two photons. In hydrogen, theoretical predictions have been limited for many years by inconsistencies of the published values for the proton charge radius that is used as input to these calculations. Even though the nuclear-size-dependent term enters only with 4 parts in 10^{10} to the transition frequency, it contributes by far the largest uncertainty. Even worse, the various values for the proton charge radii discussed in the literature disagree by several standard uncertainties.

In comparison, absolute frequency measurements in He^+ are more promising because the contributions of higher-order QED effects are larger than the uncertainty due to the nuclear charge radius. In hydrogen, the B_{60} and B_{7i} terms contribute with −8 kHz, while the uncertainty of the proton charge radius amounts to 44 kHz. In contrast, in He^+ B_{60} and B_{7i} are significantly larger and amount to −543 kHz, which is twice as large as the uncertainty due to the nucleus of 295 kHz. The corresponding values are shown in Table II. $\Delta E_{2S\text{-}1S} = E_{2S} - E_{1S}$ is the measured transition energy. We define the Lamb shifts $\mathcal{L}_{1S}$ and $\mathcal{L}_{2S}$ according to the generally adopted convention that recoil corrections, which are beyond the Dirac energy value but do not lift the $2S_{1/2}$-$2P_{1/2}$ degeneracy, as well as hyperfine effects, are *excluded* from the definition of the Lamb shift $\mathcal{L}$. Essentially, the Lamb shift is the sum of radiative corrections, effects due to the finite nuclear size and nuclear polarizability, and higher-order recoil (two-body effects) and radiative-recoil corrections. The following implicit definition [63] is the commonly adopted one, and reads

$$E = c^2 m_r [f(n,j) - 1] - \frac{c^2 m_r^2}{2(m_e + M)}[f(n,j) - 1]^2 + \mathcal{L} + E_{hfs}. \tag{21}$$

Here, E is the energy level of the bound two-body system (electron+nucleus), and $f(n,j)$ is the dimensionless Dirac energy. For example, we have $f(1,\frac{1}{2}) = f(1S) = \sqrt{1-(Z\alpha)^2}$ and $f(2,\frac{1}{2}) = f(2S) = \sqrt{\frac{1}{2}[1+\sqrt{1-(Z\alpha)^2}]}$ for the $1S$ and $2S$ states, respectively. The other symbols are as follows: $m_r(M)$ is the reduced mass of the system, and E_{hfs} is the energy shift due to hyperfine effects. The latter is absent for a spinless nucleus.

The difference in the Dirac energies, $\Delta E^{Dirac}_{2S\text{-}1S}$, can be calculated for the $1S$-$2S$ transition with an uncertainty $(\delta R_\infty/R_\infty)\Delta E^{Dirac}_{2S\text{-}1S} \approx (\delta R_\infty/R_\infty)\Delta E_{2S\text{-}1S}$ (see Table II), which is proportional to the relative uncertainty of the Rydberg constant, $\delta R_\infty/R_\infty = 6.6\times10^{-12}$ [61]. The Lamb shift difference $\mathcal{L}_{1S} - \mathcal{L}_{2S}$ can be determined to the same absolute precision in frequency units from H spectroscopy because $\Delta E_{2S\text{-}1S}$ has been measured [1] to an accuracy of 1.4×10^{-14}, much better than R_∞. Present knowledge of R_∞ comes mainly from precision spectroscopy of H($1S$-$2S$), H($2S$-$8D$), H($2S$-$12D$), and similar transitions [2]. A more elaborate version of this approach is based on the method of least squares [2,64], and

TABLE II. Comparison of H and $^4He^+$. This listing includes the transition frequency and critical contributions to the energy levels such as the Lamb shift $\mathcal{L}$, some higher-order QED terms, and the energy shifts due to the nuclear size and polarizability. Uncertainties are given in parentheses. The nuclear-size corrections are calculated with the rms charge radii $R_p=0.897(18)$ fm [58,59] for the proton and $R_\alpha=1.681(4)$ fm for the α particle [60]. The nuclear polarizability corrections are the results of calculations; see Eq. (A11) of Ref. [61] and Ref. [62] for the proton and the α particle, respectively. With regard to the potential improvement of the nuclear-size uncertainty due to the ongoing muonic hydrogen and muonic helium experiments, we note that the value in the last row for $He^+(1S\text{-}2S)$ is obtained under the additional assumption that the nuclear polarizability correction of the μ^4He $2S$ state can be calculated to 5% uncertainty.

	$H(1S\text{-}2S)$ (kHz)	$He^+(1S\text{-}2S)$ (kHz)	Z dependence
Frequencies			
$\Delta E_{2S\text{-}1S}$	2.466×10^{12}	9.869×10^{12}	Z^2
$1S\text{-}2S$ natural linewidth	0.0013	0.084	Z^6
Selected individual contributions and theoretical Lamb shift values			
Nuclear polarizability	−0.06(2)	−28(3)	
B_{60} and B_{7i} terms	−8(3)	−543(185)	$Z^{6\cdots}$
Nuclear size (for the proton and the ^{4}He nucleus)	1102(44)	62079(295)	Z^4R^2
$\mathcal{L}_{1S}-\mathcal{L}_{2S}$	7127887(44)	93856127(348)	$\approx Z^{3.7}$
Some relevant uncertainties and projected improvements			
Uncertainty due to uncalculated higher-order terms (C_{50}, recoil, etc.)	±2	±100	Z^{5-7}
Conceivable reduced uncertainty of the nuclear-size correction assuming the availability of μH and μ^4He^+ Lamb shift measurements	±2	±40	

on the assumption that all currently measured accurate transitions can be described with a single coherent theory described by quantum electrodynamics, which covers all transitions among the hydrogenic bound states.

Deriving the Rydberg constant in this way, the main relevant input parameters are the $H(1S\text{-}2S)$, $H(2S\text{-}8D)$, and $H(2S\text{-}12D)$ transitions. A measurement of the $H(1S\text{-}3S)$ transition with increased accuracy (a realistic goal is on the level of 1 kHz precision) is currently being pursued at the Max-Planck-Institute of Quantum Optics (Garching) and at the Laboratoire Kastler-Brossel in Paris. If successful, these ongoing experiments would reduce the uncertainty in R_∞ by a factor of 2, with a corresponding reduction in the contribution to the theoretical uncertainty of the He^+ frequencies due to the Rydberg constant.

Concerning the entry for $\mathcal{L}_{1S}-\mathcal{L}_{2S}$ in Table II, we note that the Lamb shift does not scale exactly as Z^4 because the leading term has an additional $\ln[(Z\alpha)^{-2}]$ dependence. Both at $Z=1$ and at $Z=2$, the dependence on Z can be approximated by a noninteger power $\approx Z^{3.7}$. For the determination of the fractional power, it is crucial to take into account the dependence of the argument of the logarithm on the fine-structure constant, and the approximate value of the exponent slightly depends on the nuclear charge number. For $Z=1,2$ the exponent is well approximated as 3.7.

The quoted theoretical uncertainties for the Lamb shift differences $\mathcal{L}_{1S}-\mathcal{L}_{2S}$ in H and He^+ take into account the recent investigations reported in Refs. [65–67] for H and in Ref. [68] for He^+. The theoretical uncertainties of these calculated Lamb shift differences result from quadratically adding the uncertainties of the nuclear-size term and computational uncertainties, where we note the reduction in the uncertainty of the nuclear-size correction for the Lamb shift difference $\mathcal{L}_{1S}-\mathcal{L}_{2S}$ by a factor of 7/8 in comparison to $\mathcal{L}_{1S}$ as taken from Table 3 of Ref. [68]. The resulting relative uncertainty in He^+ of 3.7 ppm (±348 kHz) is roughly half the size of the corresponding value in hydrogen (6.3 ppm or ±44 kHz) and is composed in almost equal parts of uncertainties in the nuclear size and computational uncertainties. This is in sharp contrast to the situation in hydrogen where no immediate progress is possible by improved calculations. The total theoretical uncertainties of the Lamb shift differences are presently a lot larger than their uncertainties due to the Rydberg constant alone (16 and 65 kHz, or 2.2 and 0.7 ppm, respectively, due to R_∞).

We now turn to a brief discussion regarding the evaluation of the theoretical Lamb shift values from QED theory. In general, the long tradition of bound-state QED computations has led to precise values for many of the higher-order terms for the one-loop and two-loop self-energies, vacuum polarization, etc., as tabulated in Ref. [57] for H and in Ref. [68] for He^+. Many of these terms were calculated to such high numerical precision that we can disregard their uncertainty in the present context, as is evident, e.g., from Table 3 of Ref. [68]. In recent years, intensive studies of the higher-order two-loop corrections to the Lamb shift (with self-energy,

vacuum polarization, and mixed graphs) have been performed with two different methods. The first of these is based on an expansion in powers of $Z\alpha$ and $\ln[(Z\alpha)^{-2}]$, with coefficients labeled as B_{40}, B_{50}, and B_{6i} with $i \in \{0,1,2,3\}$, and B_{7i} with $i \in \{0,1,2\}$, where the first index of the B coefficients labels the power of $Z\alpha$ and the second index labels the power of the logarithm $\ln[(Z\alpha)^{-2}]$ (see Ref. [66]). The second method is based on a nonperturbative (in $Z\alpha$) numerical approach [67]. The B_{6i} coefficients have turned out to be surprisingly large, with a remaining contribution to B_{60} due to high-energy virtual photons still being investigated. The convergence of this expansion is rather modest, and nonnegligible contributions from unknown B_{7i} terms cannot be excluded.

Nonperturbative all-order calculations were performed first at high Z and recently down to $Z=10$, and then extrapolated to $Z=1$. The result differs from the perturbative approach by nearly 7 kHz for the H($1S$) two-loop shift. Moreover, following common practice (see also the discussion in Ref. [66]), we take half of this discrepancy as uncertainty, resulting in the 3 kHz theoretical uncertainty quoted in Table II for the B_{60} and B_{7i} terms. Obviously, these terms become quite large for He^+ because they scale as Z^6 and higher powers. Other uncalculated effects included in the two-loop uncertainty estimate are the three-loop C_{50} term of order $\alpha^3(Z\alpha)^5$ in units of the electron mass and uncalculated higher-order recoil corrections.

The uncertainties of the nuclear radii could be reduced by a factor of 10–20 via a measurement of the $2S$-$2P$ energy difference in muonic hydrogen (denoted in the literature as μp or μH; here we use μH) and muonic helium ions (μ^4He^+), where the nuclear-size shift is an important part of the Lamb shift and can therefore be deduced with high accuracy. For μH, such a Lamb shift experiment is presently being performed at the Paul Scherrer Institute [69] using a pulsed infrared laser system ($\lambda=6$ μm, corresponding to $\Delta E_{2P\text{-}2S}=0.2$ eV). The μH experiment is very challenging for several reasons but appears to be simpler in μHe^+. The cross sections for collisional $2S$ quenching are much smaller in the case of helium as compared to muonic hydrogen, and the muon experiment can thus be performed at significantly higher gas densities. In addition there are better detectors available for 8 keV photons from $\mu He^+(2P\text{-}1S)$ transitions than for 2 keV photons.

In order to provide a historical perspective, we note that for μHe^+ red laser light (812 nm) is needed, and a $2S$-$2P$ resonance line was measured at CERN already in the 1970s [70]. The experiment [70] was based on a lifetime of the metastable μHe^+_{2S} state of at least 1 μs, but much shorter lifetimes were found by other groups at high He gas pressures [71,72]. A new laser experiment [73] was therefore initiated at low pressures, where collisional $2S$ quenching becomes negligibly small. No $\mu He^+(2S\text{-}2P)$ resonance line was found at the wavelength claimed by the previous experiment [70], which means that the search for this $2S$-$2P$ resonance is still an open task [73]. With the progress in laser technology and muon-beam intensities, such muonic Lamb shift experiments are feasible today.

A summary of transition frequencies, interesting contributions to the Lamb shift, and other data relevant to the current project is given in Table II. We note that the nuclear polarizability correction for $^4He^+$ has been computed very recently for the first time [62]. The correction is numerically significant on the precision level which may be reached in the not-too-distant future.

To conclude the discussion, we note the current theoretical prediction for the $1S$-$2S$ transition frequency in $^4He^+$, which reads

$$\nu_{1S\text{-}2S}(^4He^+) = 9\ 868\ 561\ 006.74(35)\ \text{MHz}, \qquad (22)$$

where the uncertainty is obtained by quadratically adding the Lamb shift uncertainty of ± 348 kHz and the uncertainty due to the Rydberg constant of ± 65 kHz. A measurement of the $1S$-$3S$ transition in hydrogen on the level of 1 kHz would halve the uncertainty due to R_∞. It is obvious for both H and He^+ that higher-order QED contributions can be tested on a sensitive level only when better values for the nuclear radii become available from muonic Lamb shift measurements. If we assume, furthermore, that a moderate improvement of the R_∞ uncertainty can be achieved (e.g., via a $1S$-$3S$ measurement), this will open the field for a very sensitive test of bound-state QED in the case of He^+, on the level of 50 kHz (0.5 ppm of the Lamb shift) or better. Due to the scaling of the interesting QED corrections with high powers of Z, we believe that He^+ offers promising opportunities in comparison to H. The number of theoretical digits that can be compared with experiments is currently about the same in hydrogen and He^+, but the scaling of the limiting contributions with $Z^6/Z^2=16$ means that the same higher-order QED effects are tested already with more than one digit less experimental accuracy in He^+.

VI. SUMMARY AND OUTLOOK

We have discussed the feasibility of two-photon spectroscopy of the $1S$-$2S$ transition in He^+ using xuv frequency combs generated in external enhancement cavities and the impact of such a measurement on QED tests. The spectroscopy is shown to have a number of unique features in comparison to the vast majority of precision spectroscopy experiments on trapped ions. Most importantly, we note the ionization of the "clock" transition and the lack of a narrowband laser to drive a strong cycling transition so that standard cooling and detection schemes fail.

Our analysis of the excitation and ionization dynamics shows that the power levels at 61 nm we expect ($P_{\text{xuv}} \sim 10$–100 μW) will be sufficient for spectroscopy, although tight focusing down to <10 μm and long interaction times are necessary to attain appreciable rates. This can conveniently be fulfilled by a sample of cold trapped He^+ ions. We propose to use the production of He^{2+} ions as a signature for successful excitations. Auxiliary ions are introduced into the trap that sympathetically cool the He^+ ions and also serve as "detectors" for successful excitations via secular excitation. This detection scheme is virtually background free. Anticollinear axial excitation yields the highest rates but presents a significant experimental challenge, because of the need for temporal and spatial overlap of the short light pulses with the ions. Collinear radial excitation simplifies the ex-

periment considerably but requires up to an order of magnitude more power and/or tighter focusing.

A measurement of the He^+ $1S$-$2S$ transition frequency can provide valuable input for tests of bound-state QED. Higher-order corrections which currently cannot be tested in other hydrogenic systems would be accessible, especially if more precise nuclear radii from measurements on muonic helium and an improved Rydberg constant become available. The transition frequency can currently be predicted to within 350 kHz, corresponding to a relative uncertainty of 3.5×10^{-11}, equally limited by the accuracy of the charge radius and the B_{60} and B_{7i} terms. An analysis of typical systematic errors promises uncertainties far below that level, on the order of 10^{-16}.

ACKNOWLEDGMENT

This research was supported by the DFG cluster of excellence "Munich Centre for Advanced Photonics." T.W.H. gratefully acknowledges support by the Max-Planck Foundation.

[1] M. Niering, R. Holzwarth, J. Reichert, P. Pokasov, Th. Udem, M. Weitz, T. W. Hänsch, P. Lemonde, G. Santarelli, M. Abgrall, P. Laurent, C. Salomon, and A. Clairon, Phys. Rev. Lett. **84**, 5496 (2000).

[2] B. de Beauvoir, C. Schwob, O. Acef, L. Jozefowski, L. Hilico, F. Nez, L. Julien, A. Clairon, and F. Biraben, Eur. Phys. J. D **12**, 61 (2000).

[3] H. Häffner, T. Beier, N. Hermanspahn, H. J. Kluge, W. Quint, S. Stahl, J. Verdú, and G. Werth, Phys. Rev. Lett. **85**, 5308 (2000).

[4] J. Verdu, S. Djekic, H. Haffner, S. Stahl, T. Valenzuela, M. Vogel, G. Werth, H. J. Kluge, and W. Quint, Phys. Rev. Lett. **92**, 093002 (2004).

[5] M. W. Ritter, P. O. Egan, V. W. Hughes, and K. A. Woodle, Phys. Rev. A **30**, 1331 (1984).

[6] W. Liu, M. G. Boshier, S. Dhawan, O. van Dyck, P. Egan, X. Fei, M. Grosse Perdekamp, V. W. Hughes, M. Janousch, K. Jungmann, D. Kawall, F. G. Mariam, C. Pillai, R. Prigl, G. zu Putlitz, I. Reinhard, W. Schwarz, P. A. Thompson, and K. A. Woodle, Phys. Rev. Lett. **82**, 711 (1999).

[7] U. D. Jentschura, Phys. Rev. A **69**, 052118 (2004).

[8] B. Roth, U. Fröhlich, and S. Schiller, Phys. Rev. Lett. **94**, 053001 (2005).

[9] C. Gohle, Th. Udem, M. Herrmann, J. Rauschenberger, R. Holzwarth, H. A. Schuessler, F. Krausz, and T. W. Hänsch, Nature (London) **436**, 234 (2005).

[10] R. J. Jones, K. D. Moll, M. J. Thorpe, and J. Ye, Phys. Rev. Lett. **94**, 193201 (2005).

[11] A. Ozawa, J. Rauschenberger, C. Gohle, M. Herrmann, D. R. Walker, V. Pervak, A. Fernandez, R. Graf, A. Apolonski, R. Holzwarth, F. Krausz, T. W. Hänsch, and Th. Udem, Phys. Rev. Lett. **100**, 253901 (2008).

[12] D. C. Yost, T. R. Schibli, and J. Ye, Opt. Lett. **33**, 1099 (2008).

[13] J. G. Eden, Prog. Quantum Electron. **28**, 197 (2004).

[14] Y. V. Baklanov and V. P. Chebotayev, Appl. Phys. (Berlin) **12**, 97 (1977).

[15] J. N. Eckstein, A. I. Ferguson, and T. W. Hänsch, Phys. Rev. Lett. **40**, 847 (1978).

[16] Th. Udem, R. Holzwarth, and T. W. Hänsch, Nature (London) **416**, 233 (2002).

[17] A. Bartels, C. W. Oates, L. Hollberg, and S. A. Diddams, Opt. Lett. **29**, 1081 (2004).

[18] P. Fendel, S. D. Bergeson, Th. Udem, and T. W. Hänsch, Opt. Lett. **32**, 701 (2007).

[19] M. J. Snadden, A. S. Bell, E. Riis, and A. I. Ferguson, Opt. Commun. **125**, 70 (1996).

[20] F. Lindner, W. Stremme, M. G. Schatzel, F. Grasbon, G. G. Paulus, H. Walther, R. Hartmann, and L. Struder, Phys. Rev. A **68**, 013814 (2003).

[21] S. Kim, J. Jin, Y.-J. Kim, I.-Y. Park, Y. Kim, and S.-W. Kim, Nature (London) **453**, 757 (2008).

[22] A. Ancona, F. Roesser, K. Rademaker, J. Limpert, S. Nolte, and A. Tuennermann, Opt. Express **16**, 8958 (2008).

[23] S. Witte, R. Th. Zinkstok, W. Ubachs, W. Hogervorst, and K. S. E. Eikema, Science **307**, 400 (2005).

[24] S. Cavalieri, R. Eramo, M. Materazzi, C. Corsi, and M. Bellini, Phys. Rev. Lett. **89**, 133002 (2002).

[25] R. Th. Zinkstok, S. Witte, W. Ubachs, W. Hogervorst, and K. S. E. Eikema, Phys. Rev. A **73**, 061801(R) (2006).

[26] A. Schliesser, C. Gohle, Th. Udem, and T. W. Hänsch, Opt. Express **14**, 5975 (2006).

[27] J. Tate, T. Auguste, H. G. Muller, P. Salieres, P. Agostini, and L. F. DiMauro, Phys. Rev. Lett. **98**, 013901 (2007).

[28] L. A. Lompre, A. L'Huillier, M. Ferray, P. Monot, G. Mainfray, and C. Manus, J. Opt. Soc. Am. B **7**, 754 (1990).

[29] E. J. Takahashi, Y. Nabekawa, H. Mashiko, H. Hasegawa, A. Suda, and K. Midorikawa, IEEE J. Sel. Top. Quantum Electron. **10**, 1315 (2004).

[30] U. Birnbaum and R. Schreiner, Proc. SPIE **5965**, 59650T (2005).

[31] H. Mashiko, A. Suda, and K. Midorikawa, Opt. Lett. **29**, 1927 (2004).

[32] J. I. Larruquert and R. A. M. Keski-Kuha, Appl. Opt. **41**, 5398 (2002).

[33] P. Kirkpatrick and A. V. Baez, J. Opt. Soc. Am. **38**, 766 (1948).

[34] S. Matsuyama, H. Mimura, H. Yumoto, K. Yamamura, Y. Sano, K. Endo, Y. Mori, Y. Nishino, K. Tamasaku, T. Ishikawa, M. Yabashi, and K. Yamauchi, Rev. Sci. Instrum. **76**, 083114 (2005).

[35] The tabulated transmission is higher, but in practice oxide layers reduce the transmission significantly.

[36] K. Varjú, Y. Mairesse, B. Carré, M. B. Gaarde, P. Johnsson, S. Kazamias, R. López-Martens, J. Mauritsson, K. J. Schafer, P. Balcou, A. L'huillier, and P. Salières, J. Mod. Opt. **52**, 379 (2005).

[37] M. Murakami, J. Mauritsson, A. L'Huillier, K. J. Schafer, and M. B. Gaarde, Phys. Rev. A **71**, 013410 (2005).

[38] M. Haas, U. D. Jentschura, C. H. Keitel, N. Kolachevsky, M. Herrmann, P. Fendel, M. Fischer, Th. Udem, R. Holzwarth, T. W. Hänsch, M. O. Scully, and G. S. Agarwal, Phys. Rev. A **73**, 052501 (2006).
[39] S. Wolfram, *Mathematica—A System for Doing Mathematics by Computer* (Addison-Wesley, Reading, MA, 1988).
[40] A xuv comb at 30 nm is no appropriate source, since 1*S*-2*P* is a one-photon transition, so the quasi-cw argument of a two-photon transition does not hold.
[41] A. Friedenauer, F. Markert, H. Schmitz, L. Petersen, S. Kahra, M. Herrmann, Th. Udem, T. W. Hänsch, and T. Schätz, Appl. Phys. B: Lasers Opt. **84**, 371 (2006).
[42] H. Dehmelt, Bull. Am. Phys. Soc. **20**, 60 (1975).
[43] T. Rosenband, P. O. Schmidt, D. B. Hume, W. M. Itano, T. M. Fortier, J. E. Stalnaker, K. Kim, S. A. Diddams, J. C. J. Koelemeij, J. C. Bergquist, and D. J. Wineland, Phys. Rev. Lett. **98**, 220801 (2007).
[44] S. Klarsfeld, Phys. Lett. **30A**, 382 (1969).
[45] S. R. Jefferts, C. Monroe, E. W. Bell, and D. J. Wineland, Phys. Rev. A **51**, 3112 (1995).
[46] M. A. Rowe, A. Ben-Kish, B. DeMarco, D. Leibfried, V. Meyer, J. Beall, J. Britton, J. Hughes, W. M. Itano, B. Jelenkovic, C. Langer, T. Rosenband, and D. J. Wineland, Quantum Inf. Comput. **2**, 257 (2002).
[47] J. S. Cohen and J. N. Bardsley, Phys. Rev. A **18**, 1004 (1978).
[48] D. J. Berkeland, J. D. Miller, J. C. Bergquist, W. M. Itano, and D. J. Wineland, J. Appl. Phys. **83**, 5025 (1998).
[49] G. Morigi and S. Fishman, Phys. Rev. Lett. **93**, 170602 (2004).
[50] H. Goldstein, *Classical Mechanics*, 2nd ed. (Addison-Wesley, Reading, MA, 1980), p. 672.
[51] D. J. Wineland and W. M. Itano, Phys. Rev. A **20**, 1521 (1979).
[52] G. Morigi and H. Walther, Eur. Phys. J. D **13**, 261 (2001).
[53] This was part of the consistency checks in the calculation of the spectra.
[54] H. A. Bethe and E. E. Salpeter, *Quantum Mechanics of One- and Two-Electron Atoms* (Springer, Berlin, 1977).
[55] U. D. Jentschura and M. Haas, Phys. Rev. A **78**, 042504 (2008).
[56] G. Breit, Nature (London) **122**, 649 (1928).
[57] M. I. Eides, H. Grotch, and V. A. Shelyuto, Phys. Rep. **342**, 63 (2001).
[58] P. G. Blunden and I. Sick, Phys. Rev. C **72**, 057601 (2005).
[59] I. Sick, Phys. Lett. B **576**, 62 (2003).
[60] I. Sick, Phys. Rev. C **77**, 041302(R) (2008).
[61] P. J. Mohr and B. N. Taylor, Rev. Mod. Phys. **77**, 1 (2005).
[62] K. Pachucki and A. M. Moro, Phys. Rev. A **75**, 032521 (2007).
[63] J. Sapirstein and D. R. Yennie, in *Quantum Electrodynamics*, edited by T. Kinoshita, Advanced Series on Directions in High Energy Physics Vol. 7 (World Scientific, Singapore, 1990), pp. 560–672.
[64] U. D. Jentschura, S. Kotochigova, E.-O. Le Bigot, P. J. Mohr, and B. N. Taylor, Phys. Rev. Lett. **95**, 163003 (2005).
[65] K. Pachucki and U. D. Jentschura, Phys. Rev. Lett. **91**, 113005 (2003).
[66] U. D. Jentschura, A. Czarnecki, and K. Pachucki, Phys. Rev. A **72**, 062102 (2005).
[67] V. A. Yerokhin, P. Indelicato, and V. M. Shabaev, Phys. Rev. A **71**, 040101(R) (2005).
[68] U. D. Jentschura and M. Haas, Can. J. Phys. **85**, 531 (2007).
[69] T. Nebel, F. D. Amaro, A. Antognini, F. Biraben, J. M. R. Cardoso, C. A. N. Conde, A. Dax, S. Dhawan, L. M. P. Fernandes, A. Giesen, T. W. Hänsch, P. Indelicato, L. Julien, P. E. Knowles, F. Kottmann, E. Le Bigot, Y.-W. Liu, J. A. M. Lopes, L. Ludhova, C. M. B. Monteiro, F. Mulhauser, F. Nez, R. Pohl, P. Rabinowitz, J. M. F. dos Santos, L. A. Schaller, K. Schuhmann, C. Schwob, D. Taqqu, and J. F. C. A. Veloso, Can. J. Phys. **85**, 469 (2007).
[70] G. Carboni, G. Gorini, G. Torelli, L. Palffy, F. Palmonari, and E. Zavattini, Nucl. Phys. A **278**, 381 (1977).
[71] H. von Arb, F. Dittus, H. Heeb, H. Hofer, F. Kottmann, S. Niggli, R. Schaeren, D. Taqqu, and J. Unternährer, Phys. Lett. **136B**, 232 (1984).
[72] M. Eckhause, P. Guss, D. Joyce, J. R. Kane, R. T. Siegel, W. Vulcan, R. E. Welsh, R. Whyley, R. Dietlicher, and A. Zehnder, Phys. Rev. A **33**, 1743 (1986).
[73] P. Hauser, H. P. von Arb, A. Biancchetti, H. Hofer, F. Kottmann, C. Luchinger, R. Schaeren, F. Studer, and J. Unternährer, Phys. Rev. A **46**, 2363 (1992).